Biosensors and Bioelectronics 218 (2022) 114755

Contents lists available at ScienceDirect

Biosensors and Bioelectronics

journal homepage: www.elsevier.com/locate/bios

Determination of the nanoscale electrical properties of olfactory receptor hOR1A1 and their dependence on ligand binding: Towards the development of capacitance-operated odorant biosensors

Anna Lagunas [a,b,*], Christine Belloir [c], Loïc Briand [c], Pau Gorostiza [b,a,d], Josep Samitier [b,e,a,**]

[a] Biomedical Research Networking Center in Bioengineering, Biomaterials, and Nanomedicine (CIBER-BBN), av. Monforte de Lemos, 3-5. Pabellón 11. Planta 0, 28029, Madrid, Spain
[b] Institute for Bioengineering of Catalonia (IBEC), Barcelona Institute of Science and Technology, c/Baldiri i Reixac 10-12, 08028, Barcelona, Spain
[c] Centre des Sciences du Goût et de l'Alimentation, CNRS, INRAE, Institut Agro Dijon, Université Bourgogne Franche-Comté, 9E Bd Jeanne d'Arc, 21000, Dijon, France
[d] Catalan Institution for Research and Advanced Studies (ICREA), pg. Lluís Companys 23, Barcelona, 08010, Spain
[e] Department of Electronics and Biomedical Engineering, Faculty of Physics, University of Barcelona (UB), c/Martí i Franquès 1, 08028, Barcelona, Spain

ARTICLE INFO

Keywords:
Olfactory receptors (ORs)
Odorant binding
Electrochemical scanning tunneling microscopy (EC-STM)
Open-circuit voltage (V_{OC})

ABSTRACT

The transduction of odorant binding into cellular signaling by olfactory receptors (ORs) is not understood and knowing its mechanism would enable developing new pharmacology and biohybrid electronic detectors of volatile organic compounds bearing high sensitivity and selectivity. The electrical characterization of ORs in bulk experiments is subject to microscopic models and assumptions. We have directly determined the nanoscale electrical properties of ORs immobilized in a fixed orientation, and their change upon odorant binding, using electrochemical scanning tunneling microscopy (EC-STM) in near-physiological conditions. Recordings of current versus time, distance, and electrochemical potential allows determining the OR impedance parameters and their dependence with odorant binding. Our results allow validating OR structural-electrostatic models and their functional activation processes, and anticipating a novel macroscopic biosensor based on ORs.

1. Introduction

Olfactory receptors (ORs) comprise the largest multigene family in the vertebrates, with about 400 genes identified in humans (Buck and Axel, 1991; Malnic et al., 2004). They are expressed primarily by olfactory sensory neurons located in the olfactory epithelium in the nasal cavity and are responsible for odorant detection. Moreover, the expression of ORs in other tissues have been reported, where they exert distinct biological functions (Lee et al., 2019; Orecchioni et al., 2022). Despite the growing evidence that ORs are essential in relevant biological processes such as chemotaxis in immune response, wound healing, and cancer, there is a shortage of rapid and ultrasensitive analytical methods to detect odorant molecules. ORs belong to the class A (rhodopsin-like) family of G protein-coupled receptors (GPCRs) and around half of the GPCRs are ORs. GPCRs are the most abundant membrane proteins having widespread, significant roles in signal transduction in cells. Therefore, they are a major pharmacological target, with approximately the 40% of approved drugs on the market targeting GPCRs (Hauser et al., 2017; Hutchings et al., 2017).

The mechanism of olfactory transduction in the main olfactory epithelium involves OR switching from a conformationally inactive state towards an active state upon odorant binding, which couples with the intracellular G protein G_{olf} and activates adenylyl cyclase type-III. This leads to an increase of the intraciliary level of cyclic adenosine monophosphate (cAMP) opening cyclic-nucleotide-gated (CNG) non-selective cation channels. The subsequent ionic flux causes membrane depolarization, the activation of Na^+-channels and consequently, action potential firing (Boccaccio, 2018). ORs show high selectivity and sensitivity towards odorant detection (Bhandawat et al., 2010; Bohbot and Vernick, 2020), a characteristic that prompted the development of biohybrid sensors using ORs for the detection of volatile organic compounds (Yamada et al., 2021; Yang et al., 2017).

* Corresponding author. Institute for Bioengineering of Catalonia (IBEC), Barcelona Institute of Science and Technology, c/Baldiri Reixac 10-12, 08028, Barcelona, Spain.
** Corresponding author. Institute for Bioengineering of Catalonia (IBEC), Barcelona Institute of Science and Technology, c/Baldiri i Reixach 10-12, 08028, Barcelona, Spain.
E-mail addresses: alagunas@ibecbarcelona.eu (A. Lagunas), jsamitier@ibecbarcelona.eu (J. Samitier).

https://doi.org/10.1016/j.bios.2022.114755
Received 9 June 2022; Received in revised form 9 September 2022; Accepted 23 September 2022
Available online 28 September 2022

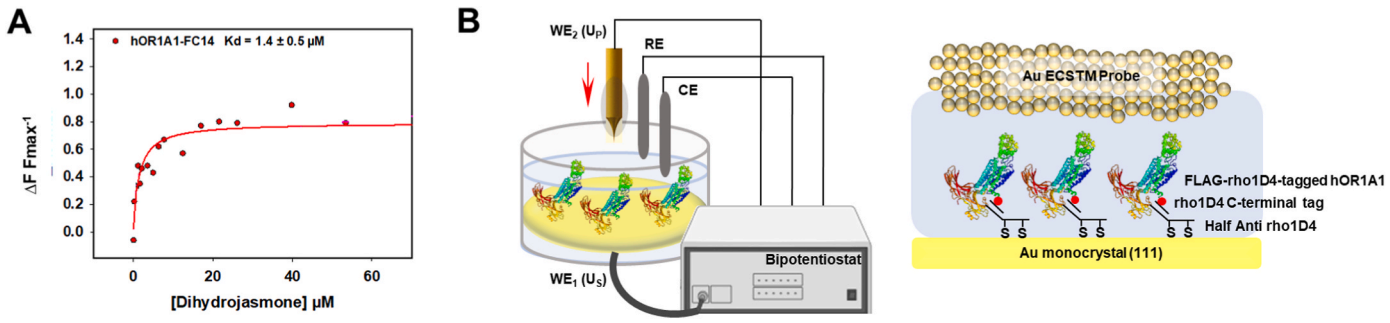

Fig. 1. (A) Binding activity of purified hOR1A1 using intrinsic tryptophan fluorescence. Dose-response relationship of hOR1A1 fluorescence (λexc = 280 nm, λem = 340 nm) following dihydrojasmone application. The data were fitted with sigmoid dose-response curves and K_d value obtained (mean ± s.d, N = 3). (B) Schematic representation of the experimental set-up in the EC-STM. hOR1A1 was selectively immobilized through its C-terminal tag Rho1D4, thus providing homogenous orientation of the receptor. Due to lack of any crystalline structure for hOR1A1, sequence homology with Phyre2 has been used for the receptor representation. Abbreviations: WE, working electrode; RE, reference electrode; CE, counter electrode.

Among the non-optical methods for the detection of volatile organic compounds, the electronic sensing devices termed "E-noses" were found particularly suitable due to their sensitivity, low cost of manufacture and ease of use. Some graphene-based E-noses reported detection limits below parts per trillion, while others based on field-effect transistors showed a detection limit in the low parts per billion (ppb) range. The main drawback of E-noses are their low specificity. Conversely, the "bioelectronic noses" combining ORs with solid-state electronic transducers enable the intrinsically selective detection of odorants and the transduction of the chemical signal into an electronic readout (Bohbot and Vernick, 2020). Changes in conductance/resistance are measured in response to odorant binding with ORs-based biosensors, and sensitivity values have been reported down to femtomolar concentrations for solubilized odorants and down to ppb for gas analysis (Bohbot and Vernick, 2020; Khadka et al., 2020; Yamada et al., 2021). However, the quantitative aspects of odorant detection remain largely unknown, thus hampering the further development of odorant biosensors.

This made the electrical characterization of ORs a subject of interest, which has been mainly addressed by electrochemical impedance spectroscopy (EIS) in bulk experiments (Hou et al., 2007; Khadka et al., 2019). Recent findings suggest that ligand recognition by ORs could be determined by the nanoscale alterations of charge distribution in the receptor structure. However, the electrical characterization of ORs and their response towards ligand binding in bulk experiments is subject to microscopic models and assumptions. These models are generally based on equivalent impedance networks trying to link the dipoles and charges of the backbone and side chains of the receptor in its native and activated state, with the experimental results obtained (Alfinito et al., 2015; Alfinito and Reggiani, 2016). Measuring the electrical changes associated to ligand-receptor interactions requires of a tightly regulated set-up and nanometric precision to fix receptor orientation, thus providing a selective and quantifiable response. Here, we have directly determined the nanoscale electrical properties of human OR hOR1A1 in the presence of its cognate ligand dihydrojasmone, using electrochemical scanning tunneling microscopy (EC-STM) under bipotentiostatic control. In particular, we have measured current-voltage (*I–V*), current-time (*I-t*) and current-distance (*I-z*) characteristics (Fig. S1) of the receptor immobilized in a fixed orientation in a near-physiological environment. Results show that ORs behave as parallel resistor-capacitor (RC) circuits with R and C decreasing by 20% upon ligand binding. To highlight the implications of our results at the macroscopic scale, we extended our single-protein conductance measurements to large-area current recordings, which are widely accessible. Our results pave the way towards the development of better biohybrid odorant sensors with application to detect volatile analytes and will allow validating OR structural-electrostatic models and their functional activation.

2. Results and discussion

2.1. Receptor immobilization

hOR1A1 was overexpressed in a stable tetracycline inducible HEK293S GnTI$^-$ cell line as previously described (Belloir et al., 2017). The receptor was engineered by inserting the epitope tags rho1D4 at the C-terminal and FLAG at the N-terminal to allow its purification and detection. Circular dichroism analysis demonstrated that detergent-solubilized FLAG-rho1D4-tagged hOR1A1was properly folded into α-helical structure, as expected for the secondary structures of a GPCR (Erdogmus et al., 2019). Receptor functionality was assessed by ligand binding using an intrinsic tryptophan fluorescence assay, which revealed the receptor bound its cognate odorant, dihydrojasmone, with an affinity in the micromolar range exhibiting a K_d value of 1.4 ± 0.5 µM (Fig. 1A).

A uniform orientation of the receptor is essential in single molecule experiments (Lagunas et al., 2018; López-Ortiz et al., 2022). To achieve it hOR1A1 was immobilized on the Au(111) electrode of the EC-STM by half anti-Rhodopsin antibody, against the C-terminal tag Rho1D4 (Sharma and Mutharasan, 2013), (Fig. 1B). Coverage of the substrate was monitored by atomic force microscopy (AFM) imaging (Fig. S2). Height histograms show a peak centered at 4.8 ± 0.9 nm after the incubation with the hOR1A1, which was attributed to the receptor, in agreement with the sequence homology data obtained for hOR1A1 (Kelley et al., 2015).

2.2. Conductance measurements

Single-protein current-bias voltage (*I–V*) characteristics of hOR1A1 were measured in a physiological environment (50 mM phosphate buffer pH 7.4) by EC-STM. The experiments were conducted under bipotentiostatic control of the probe and sample electrodes versus an Ag/AgCl (SSC) reference electrode, with and without the presence of dihydrojasmone. *I–V* measurements were performed at a fixed separation between the probe and sample (given by a setpoint current of 0.4 nA) to avoid physical contact between the STM probe and the protein (Artés et al., 2012a). The STM feedback loop allowed fixing the setpoint current and it was turned off during 0.86 s to perform each *I–V* recording at a rate of 581 mV s^{-1}. This avoids the biasing that might be introduced by the contact geometry in contact mode (Zhang et al., 2019), and provides a more flexible configuration.

Sample potential (U_S) and initial probe potential (initial U_P) were set at 0.25 V and 0.45 V, respectively. Faradaic leakage current was maintained below a few pA through probe insulation (Artés et al., 2012b). To obtain each *I–V* plot, the probe was positioned over the sample at a current set point of 0.4 nA, the feedback loop disconnected and the probe current recorded while a voltage ramp is applied to the EC-STM

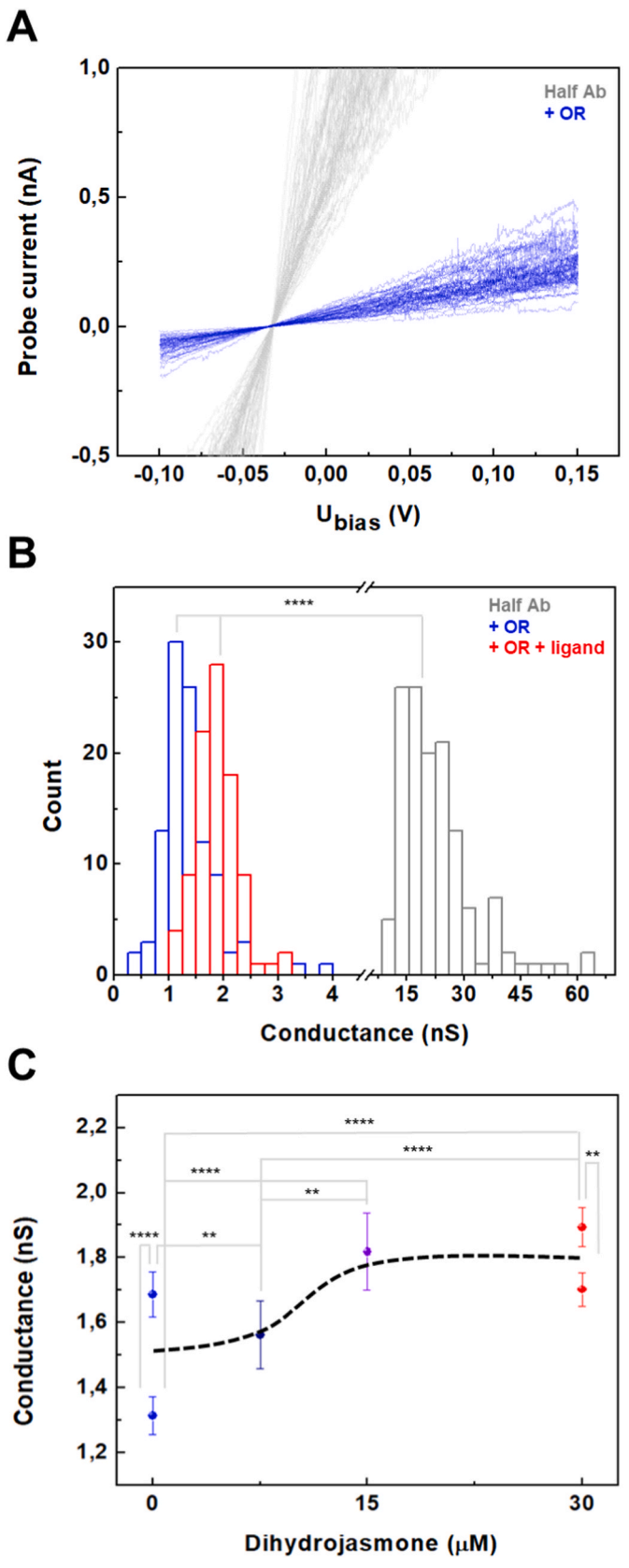

(caption on next column)

Fig. 2. (A) Ensemble of EC-STM current-bias voltage (*I–V*) curves obtained for half anti-Rhodopsin (grey) and hOR1A1 (blue), showing the decrease in conductance upon receptor immobilization. (B) Conductance histograms obtained from the linear fitting of individual *I–V* curves for half anti-Rhodopsin (grey), hOR1A1 before (blue) and after incubation with 30 μM dihydrojasmone (red). (C) Plot of the conductance variation in hOR1A1with the increasing dihydrojasmone concentration: 0 μM (blue), 7.5 μM (navy), 15 μM (purple) and 30 μM (red). Dashed black lines are an eye-guide. Values are the mean ± SE. n = 150. *P < 0.03, **P < 0.01, ****P < 0.0001. Experiments were conducted at a constant sample potential (U_S) of 250 mV, current set point = 0.4 nA, 50 mM sodium phosphate buffer, pH 7.4.

probe. Up to 150 *I–V* curves were recorded at different sample positions by sweeping the probe potential back and forth from 0.15 to 0.40 V (bias ($U_{bias} = U_P$-U_S) = −0.10 to 0.15 V), covering a physiological range of cell membrane potential (Kandel et al., 2000).

I–V measurements of half anti-Rhodopsin antibody alone, and hOR1A1 immobilized through half anti-Rhodopsin antibody are shown in Fig. 2A. The presence of hOR1A1 caused a pronounced reduction of conductance. We observed a linear *I–V* response in all cases; thus, a single conductance value (fitted *I–V* slope) can be assigned to each *I–V* trace. Fig. 2B shows measured distributions of the conductance values obtained for anti-Rhodopsin antibody, and hOR1A1 immobilized through half anti-Rhodopsin antibody with and without the presence of the OR cognate ligand dihydrojasmone at 30 μM concentration. The presence of the ligand caused a significant increase of conductance in hOR1A1.

To exclude contributions from the media in the gap between the probe and the sample, we conducted static break junction experiments (Artés et al., 2012b; Ruiz et al., 2017). With the feedback loop transiently disconnected, we recorded current vs. time (*I-t*) at a constant bias of 0.2 V (U_S = 0.25 V and U_P = 0.45V) and at a current set point of 0.3 nA. Spontaneous contact between the probe and the sample results in jumps (*blinks*) of the current that last as much as the contact does (Fig. S3A). They represent solely the net conductance flowing through the receptor, thus without the contribution of the media. By collecting the *blinks* with subtracted current baseline and setting them to a common time origin, 2D-*blinking* maps were built. These maps show the variability in conductance that is introduced by the geometry of the contact (Fig. S3B). Taking the most probable conductance peak, we observed that binding to dihydrojasmone caused a conductance increase (Fig. S3C) as in *I–V* non-contact measurements. In general, conductance values obtained in *I-t* measurements are lower, as expected from the more resistive environment of the protein.

Treatment with increasing concentrations of dihydrojasmone (0–30 μM) lead to a growth of conductance (Fig. 2C). Fitting the data using Hill sigmoidal equation with variable slope (i.e., 4 parameters logistical) (Fig. S4) yielded an EC50 of 11.2 μM, in agreement with previous results (Belloir et al., 2017), and thereby validating our EC-STM set-up for studying hOR1A1-dihydrojasmone binding. A Hill coefficient of 9.9 was obtained from the fit indicating a non-linear relation between de EC-STM response and odorant concentration. Supralinear relation (i.e., Hill coefficient >1) has been previously reported for ORs and attributed to repeated binding (Bhandawat et al., 2005; Sanmartí-Espinal et al., 2017).

We also conducted current-distance (*I-z*) measurements on hOR1A1 in the absence/presence of dihydrojasmone at the same concentrations used in *I–V* experiments (Fig. S5). *I-z* measurements were conducted as previously described (Artés et al., 2011; Lagunas et al., 2018) at a current set point of 0.4 nA, and at a constant bias of 0.2 V (U_S = 0.25 V and U_P = 0.45V). Up to 100 *I-z* curves were recorded per sample and distance decay factors (β) were quantified from individual semi-logarithmic *I-z* plots. We observed that β decreases with the increasing dihydrojasmone concentration, suggesting that dihydrojasmone increases the spatial span of the hOR1A1 currents.

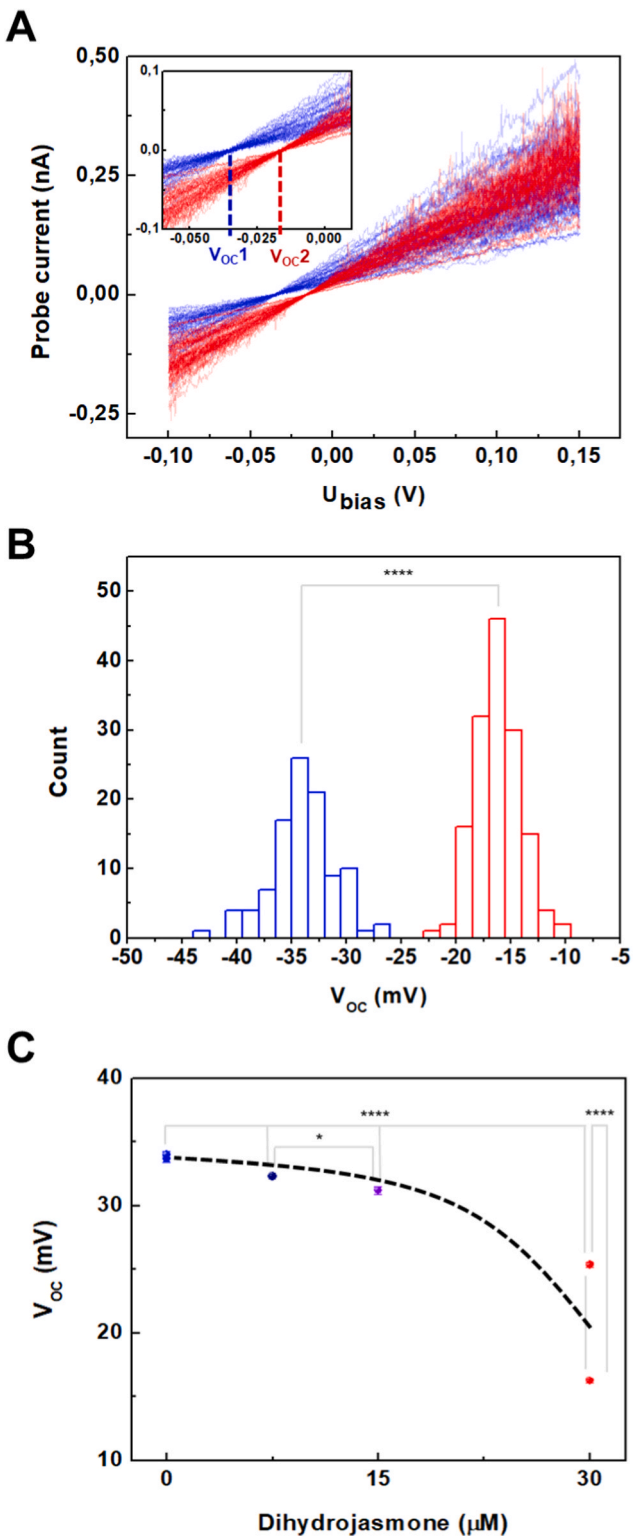

Fig. 3. (A) Superimposition of *I–V* curves from hOR1A1 before (blue) and after (red) incubation with 30 μM dihydrojasmone ligand. Dihydrojasmone causes a shift towards a lower absolute value of the open-circuit voltage (V_{OC}), inset. (B) V_{OC} histograms obtained from the linear fitting of individual *I–V* curves in A. (C) Plot of the V_{OC} variation (absolute values) in hOR1A1with the increasing dihydrojasmone concentration: 0 μM (blue), 7.5 μM (navy), 15 μM (purple) and 30 μM (red). Dashed black lines are an eye-guide. Values are the mean ± SE. n = 150. *P < 0.03, **P < 0.01, ****P < 0.0001. Experiments were conducted at a constant sample potential (U_S) of 250 mV, current set point = 0.4 nA, 50 mM sodium phosphate buffer, pH 7.4.

2.3. Capacitive behavior of OR

Besides the conductance increase, *I–V* curves showed a shift of around 20 mV in the open-circuit voltage (V_{OC}) towards lower potentials (absolute values) in the presence of dihydrojasmone (Fig. 3A), which is not observed in the absence of the ligand (Fig. S6A). The V_{OC} value obtained from the *I–V* curves for the hOR1A1 was 33.8 ± 0.2 mV, which was similar to that obtained for the half anti-Rhodopsin antibody alone (V_{OC} = 31.5 ± 0.2 mV) and significantly higher (P < 0.0001) than that obtained for hOR1A1 with dihydrojasmone at 30 μM concentration (V_{OC} = 21.8 ± 0.3 mV; Fig. 3B). This indicates that ligand binding produces a decrease in the receptor potential. Treatment with increasing concentrations of dihydrojasmone (0–30 μM) caused V_{OC} to decrease exponentially with a 1/e of 12.8 μM (Fig. 3C and S6B).

To further confirm the effects of ligand binding, we conducted *I–V* measurements of the receptor after flash-freezing in N_2 liquid and −80 °C storage, which produces a decrease in the receptor functionality (Fig. S7A). In this case, we observed that the loss of receptor activity translates in no significant changes in the measured V_{OC} after treatment with dihydrojasmone 30 μM (Fig. S7B), indicating that the shift of the V_{OC} to lower potentials is related to the electrostatic interaction of the binding between dihydrojasmone and hOR1A.

The existence of a V_{OC} different than zero in the experimental results suggests that hOR1A1 acts as an electrical first order system to a voltage ramp. Reported EIS measurements in bulk showed that ligand binding in ORs can be monitored following the variation of the impedance spectra. Nyquist plots were fitted using a modified Randles equivalent circuit, in which the response of the receptor was essentially described by the impedance of the Rp-CPE parallel circuit (Alfinito et al., 2010). In agreement with that, we modeled the electrical behavior of hOR1A1 as an RC parallel circuit (Fig. 4A), and empiric impedance values were directly determined, resulting in R_1 = 583 MΩ, C_1 = 0.10 nF (Supporting information). The interaction of OR with dihydrojasmone produces a decrease around 11% of the resistive part, and around 30% of the capacitive part of the electrical equivalent circuit (from 583 MΩ to 517 MΩ, and from 0.10 nF to 0.07 nF, respectively. See Supporting information). To highlight the implications of these results at the macroscopic scale, we extended the measurements to large-area current recordings, which are widely available. We conducted cyclic voltammetry (CV) measurements in bulk. hOR1A1 was selectively immobilized on a gold electrode through half anti-Rhodopsin antibody in analogy to the EC-STM experimental set-up, thus providing a uniform receptor orientation. Measurements were performed in the absence/presence of dihydrojasmone, and the corresponding specific capacitance was determined as previously described (Wang et al., 2015). In agreement with EC-STM results, the specific capacitance calculated from the CVs also decreases around a 30% in the presence of the ligand at different scan rates (Fig. 4B and Table S1).

3. Conclusion

hOR1A1 impedance parameters and their dependence with odorant binding have been determined by EC-STM and reproduced in bulk measurements, allowing us to devise the first capacitance-operated odorant biosensor.

Biohybrid odorant sensors have been developed reporting sensitivity values in the femtomolar range (Khadka et al., 2020). Although changes in conductance/resistance are measured in response to odorant binding, the microscopic interpretation of odorant detection remains elusive and relies on theoretical models of the electric properties of ORs (Alfinito et al., 2015; Alfinito and Reggiani, 2016). To achieve full control on odorant biosensors' characteristics and improve performance, a more detailed insight on the quantitative aspects behind odorant detection is needed. Measuring the change in the electrical properties due to ligand-receptor interactions requires to fix receptor orientation and nanometric precision to produce a selective and quantifiable response.

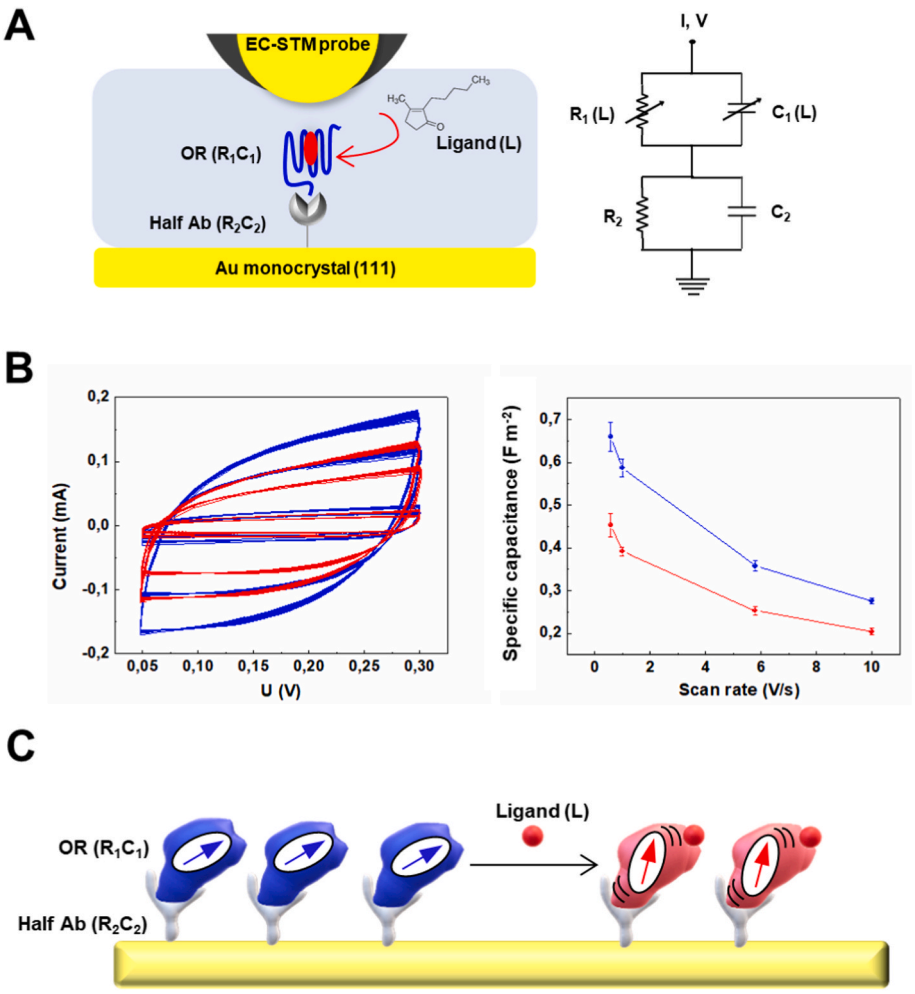

Fig. 4. (A) Electrical equivalent model proposed: a combination of RC parallel circuits for the OR (R_1C_1) and the half antibody (R_2C_2). The values of R1 and C1 are regulated by the ligand concentration. (B) Specific capacitance (right) calculated from CV (left) also show a decrease of around a 30% in the presence of the ligand at different scan rates. Values are the mean ± SE. n = 50. (C) Ligand binding induces a depolarization of the receptor that causes a decrease in the impedance.

Here, we have directly determined the nanoscale electrical properties of hOR1A1 with unprecedented control over the receptor orientation, and their change upon odorant binding, using EC-STM in near-physiological conditions. We have found that dihydrojasmone binding to the receptor causes an increase in conductance that can be measured from both *I–V* and *I-t* recordings, and which is dose dependent. The EC_{50} of 11.2 μM determined is within the range of EC_{50} values previously reported for hOR1A1 (Belloir et al., 2017), thus indicating that changes in conductance are correlated with ligand binding. Strikingly, dihydrojasmone binding produces a shift in V_{OC} towards lower potentials, which is sensible to alterations in the receptor activity.

Ligand binding in GPCRs is associated to a charge reorganization within the protein structure (Mafi et al., 2022), and analogies have been reported between some GPCRs and ORs activation mechanisms (de March et al., 2015). Therefore, and in agreement with the microscopic model proposed by Alfinito et al. for ORs (Alfinito et al., 2011), we reasoned that the changes found in the electrical properties of hOR1A1 could be attributed to the alteration of charge distribution upon dihydrojasmone binding. Ligand binding induces a depolarization of the receptor (Fig. 4C), causes a decrease in the impedance and facilitates charge transfer, as demonstrated by *I-z* measurements, increasing conductance and spatially extending (reducing) the β decay rate (Choi et al., 2008; Kumar et al., 2016; Lagunas et al., 2018; Sepunaru et al., 2015; Yan et al., 2013).

The dependence of both conductance and V_{OC} with ligand concentration agrees with the proposed mechanism of activation of GPCRs, for which a complex series of conformationally stable intermediates have been described to evolve towards a more active state with the increasing ligand concentration (Kobilka and Deupi, 2007). Finally, the simultaneous measurement of RC equivalent by means of the V_{OC} potential allows increasing the electrical sensitivity at single receptor level for biosensing applications. The electric model and fit predicts that faster *I–V* ramps would provide even larger V_{OC} shifts and thus higher ligand sensitivity both for fundamental and sensing applications.

EC-STM proved as a reliable technique to study the electrical properties of hOR1A1. The changes induced by ligand binding in conductance and specially in V_{OC} values, pave the way towards the development of better biohybrid odorant sensors with application to detect volatile analytes and to study the intriguing physiology of ORs.

CRediT authorship contribution statement

Anna Lagunas: Term, Conceptualization, Methodology, Software, Validation, Formal analysis, Investigation, Resources, Writing – original draft, Writing – review & editing, Visualization, Supervision, Project administration. **Christine Belloir:** Methodology, Validation, Formal analysis, Investigation, Resources, Writing – review & editing, Visualization. **Loïc Briand:** Methodology, Validation, Resources, Writing – review & editing, Visualization, Supervision, Funding acquisition. **Pau Gorostiza:** Conceptualization, Methodology, Resources, Writing –

original draft, Writing – review & editing, Supervision, Funding acquisition. **Josep Samitier:** Conceptualization, Resources, Writing – original draft, Writing – review & editing, Supervision, Funding acquisition.

Declaration of competing interest

The authors declare that they have no known competing financial interests or personal relationships that could have appeared to influence the work reported in this paper.

Data availability

Data will be made available on request.

Acknowledgements

This work was supported by the Biomedical Research Networking Center (CIBER), Spain. CIBER is an initiative funded by the VI National R&D&i Plan 2008–2011, Iniciativa Ingenio 2010, Consolider Program, CIBER Actions, and the Instituto de Salud Carlos III, with the support of the European Regional Development Fund (ERDF). This work was funded by the CERCA Program and by the Commission for Universities and Research of the Department of Innovation, Universities, and Enterprise of the Generalitat de Catalunya [grant numbers 2017-SGR-1079, and 2017-SGR-1442] and the project Clúster Emergent del Cervell Humà (CECH) [grant number 001-P-001682], which was cofinanced by the European Funding for Regional Economic Development (FEDER) within the framework of the ERDF Operational Program of Catalonia 2014–2020. This work was supported by grants from the Conseil Régional Bourgogne Franche-Comté (PARI grant) and the FEDER. This research also received funding from the European Union Research and Innovation Programme Horizon 2020 through the projects Human Brain Project SG3 [grant number 945539] and DEEPER [grant number ICT-36-2020–101016787], and from the Spanish Ministry of Economy and Competitiveness [grant number PID 2019-111493RB-I00]. The authors also acknowledge Dr. Albert Cortijos Aragonés for help with *I-t* measurements and data analysis, Prof. Manel Puig for help with the RC parallel circuit calculations, and Prof. Elvira Gómez for help in the interpretation of voltammetry results.

Appendix A. Supplementary data

Supplementary data to this article can be found online at https://doi.org/10.1016/j.bios.2022.114755.

References

Alfinito, E., Millithaler, J.F., Reggiani, L., Zine, N., Jaffrezic-Renault, N., 2011. RSC Adv. 1, 123–127.
Alfinito, E., Pennetta, C., Reggiani, L., 2010. SENSOR. ACTUAT. B-CHEM. 146, 554–558, 2010.
Alfinito, E., Pousset, J., Reggiani, L., 2015. J. Phys.: Conf. Ser. 647, 012002.
Alfinito, E., Reggiani, L., 2016. Phys. Rev. E 93, 062401.
Artés, J.M., Díez-Pérez, I., Gorostiza, P., 2012b. Nano Lett. 12, 2679–2684.
Artés, J.M., Díez-Pérez, I., Sanz, F., Gorostiza, P., 2011. ACS Nano 5, 2060.
Artés, J.M., López-Martínez, M., Giraudet, A., Díez-Pérez, I., Sanz, F., Gorostiza, P., 2012a. J. Am. Chem. Soc. 134, 20218–20221.
Belloir, C., Miller-Leseigneur, M.-L., Neiers, F., Briand, L., Le Bon, A.-M., 2017. Protein expr. Purif 129, 31–43.
Bhandawat, V., Reisert, J., Yau, K.-W., 2005. Science 308, 1931–1934.
Bhandawat, V., Reisert, J., Yau, K.-W., 2010. Proc. Natl. Acad. Sci. U.S.A. 107, 18682–18687.
Bohbot, J.D., Vernick, S., 2020. Biosensors 10, 26.
Boccaccio, A., 2018. Patch-clamp recordings from mouse olfactory sensory neurons. In: Simoes de Souza, F.M., Antunes, G. (Eds.), Olfactory Receptors. Methods and Protocols (Methods in Molecular Biology, 1820). Humana Press, New Jersey, pp. 113–122.
Buck, L., Axel, R.A., 1991. Cell 65, 175–187.
Choi, S.H., Kim, B., Frisbie, C.D., 2008. Science 320, 1482–1486.
Erdogmus, S., Storch, U., Danner, L., Becker, J., Winter, M., Ziegler, N., Wirth, A., Offermanns, S., Hoffmann, C., Gudermann, T., Mederos y Schnitzler, M., 2019. Nat. Commun. 10, 5784.
Hauser, A.S., Attwood, M.M., Rask-Andersen, M., Schiöth, H.B., Gloriam, D.E., 2017. Nat. Rev. Drug Discov. 16, 829–842.
Hou, X., Jaffrezic-Renault, N., Martelet, C., Zhang, A., Minic-Vidic, J., Gorojankina, T., Persuy, M.-A., Pajot-Augy, E., Salesse, R., Akimov, V., Reggiani, L., Pennetta, C., Alfinito, E., Ruiz, O., Gomila, G., Samitier, J., Errachid, A., 2007. Biosens. Bioelectron. 22, 1550–1555.
Hutchings, C.J., Koglin, M., Olson, W.C., Marshall, F.H., 2017. Nat. Rev. Drug Discov. 16, 787–810.
Kandel, E.R., Schwartz, J.H., Jessell, T.M., 2000. Principles of Neural Science. McGraw-Hill, New York.
Kumar, K.S., Pasula, R.R., Lim, S., Nijhuis, C.A., 2016. Adv. Mater. 28, 1824–1830.
Kelley, L., Mezulis, S., Yates, C., Wass, M.N., Sternberg, M.J.E., 2015. Nat. Protoc. 10, 845–858.
Khadka, R., Aydemir, N., Carraher, C., Hamiaux, C., Colbert, D., Cheema, J., Malmström, J., Kralicek, A., Travas-Sejdic, J., 2019. Biosens. Bioelectron. 126, 207–2013.
Khadka, R., Carraher, C., Hamiaux, C., Travas-Sejdic, J., Kralicek, A., 2020. Biosens. Bioelectron. 153, 112040.
Kobilka, B.K., Deupi, X., 2007. Trends Pharmacol. Sci. 28, 397–406.
Lagunas, A., Guerra-Castellano, A., Nin-Hill, A., Díaz-Moreno, I., De la Rosa, M.A., Samitier, J., Rovira, C., Gorostiza, P., 2018. Nat. Commun. 9, 5157.
Lee, S.-J., Depoortere, I., Hatt, H., 2019. Nat. Rev. Drug Discov. 18, 116–138.
López-Ortiz, M.L., Zamora, R.A., Giannotti, M.I., Hu, C., Croce, R., Gorostiza, P., 2022. Small 18, 2104366.
Mafi, A., Kim, S.K., Goddard III, W.A., 2022. Proc. Natl. Acad. Sci. U. S. A. 119, e2110085119.
Malnic, B., Godfrey, P.A., Buck, L.B., 2004. Proc. Natl. Acad. Sci. USA 101, 2584–2589.
de March, C.A., Yu, Y., Ni, M.J., Adipietro, K.A., Matsunami, H., Ma, M., Golebiowski, J., 2015. J. Am. Chem. Soc. 137, 8611–8616.
Orecchioni, M., Kobiyama, K., Winkels, H., Ghosheh, Y., McArdle, S., Mikulski, Z., Kiosses, W.B., Fan, Z., Wen, L., Jung, Y., Roy, P., Ali, A.J., Miyamoto, Y., Mangan, M., Makings, J., Wang, Z., Denn, A., Vallejo, J., Owens, M., Durant, C.P., Braumann, S., Mader, N., Li, L., Matsunami, H., Eckmann, L., Latz, E., Wang, Z., Hazen, S.L., Ley, K., 2022. Science 375, 214–221.
Ruiz, M.P., Aragonès, A.C., Camarero, N., Vilhena, J.G., Ortega, M., Zotti, L.A., Pérez, R., Cuevas, J.C., Gorostiza, P., Díez-Pérez, I., 2017. J. Am. Chem. Soc. 139, 15337.
Sanmartí-Espinal, M., Iavicoli, P., Calò, A., Taulés, M., Galve, R., Marco, M.P., Samitier, J., 2017. Sci. Rep. 7, 17483.
Sepunaru, L., Refaely-Abramson, S., Lovrinčić, R., Gavrilov, Y., Agrawal, P., Levy, Y., Kronik, L., Pecht, I., Sheves, M., Cahen, D., 2015. J. Am. Chem. Soc. 137, 9617–9626.
Sharma, H., Mutharasan, R., 2013. Anal. Chem. 85, 2472–2477.
Wang, C.-M., Wen, C.-Y., Chen, Y.-C., Chang, J.-Y., Ho, C.-W., Kao, K.-S., Shih, W.-C., Chiu, C.-M., Shen, Y.-A., 2015. The influence of specific surface area on the capacitance of the carbon electrodes supercapacitor. In: The Proceedings of the 2nd International Conference on Industrial Application Engineering, pp. 439–442, 3.
Yamada, T., Sugiura, H., Mimura, H., Kamiya, K., Osaki, T., Takeuchi, S., 2021. Sci. Adv. 7, eabd2013.
Yan, H., Bergren, A.J., McCreery, R., Della Rocca, M.L., Martin, P., Lafarge, P., Lacroix, J. C., 2013. Proc. Natl. Acad. Sci. U.S.A. 110, 5326–5330.
Yang, H., Kim, D., Kim, J., Moon, D., Song, H.S., Lee, M., Hong, S., Park, T.H., 2017. ACS Nano 11, 11847–11855.
Zhang, B., Song, W., Pang, P., Lai, H., Chen, Q., Zhang, P., Lindsay, S., 2019. Proc. Natl. Acad. Sci. USA 26, 5886–5891.